Separation Science and Technology
Publication details, including instructions for authors and subscription information:
http://www.informaworld.com/smpp/title~content=t713708471

Activated Carbons from Lignin: Their Application in Liquid Phase Adsorption

L. M. Cotoruelo[a]; M. D. Marqués[a]; F. J. Díaz[a]; J. Rodríguez-Mirasol[a]; T. Cordero[a]; J. J. Rodríguez[b]
[a] Departamento de Ingeniería Química, Universidad de Málaga, Málaga, España [b] Ingeniería Química, Universidad Autónoma de Madrid, Madrid, España

To cite this Article Cotoruelo, L. M. , Marqués, M. D. , Díaz, F. J. , Rodríguez-Mirasol, J. , Cordero, T. and Rodríguez, J. J.(2007) 'Activated Carbons from Lignin: Their Application in Liquid Phase Adsorption', Separation Science and Technology, 42: 15, 3363 — 3389
To link to this Article: DOI: 10.1080/01496390701626800
URL: http://dx.doi.org/10.1080/01496390701626800

Separation Science and Technology, 42: 3363–3389, 2007

ISSN 0149-6395 print/1520-5754 online
DOI: 10.1080/01496390701626800

Activated Carbons from Lignin: Their Application in Liquid Phase Adsorption

L. M. Cotoruelo, M. D. Marqués, F. J. Díaz, J. Rodríguez-Mirasol, and T. Cordero
Departamento de Ingeniería Química, Universidad de Málaga, Málaga, España

J. J. Rodríguez
Ingeniería Química, Universidad Autónoma de Madrid, Madrid, España

Abstract: The extent of the methylene blue (MB) adsorption from an aqueous solution is a convenient indicator in the evaluation of activated carbons. The adsorption of MB (cationic dye) from aqueous solution has been studied using twenty activated carbons. The activated carbons were prepared from acid-precipitated eucalyptus kraft lignin following a two-step process consisting of CO_2 partial gasification after carbonization in N_2 atmosphere. The adsorbed amount was studied as a function of the contact time, temperature, pH, concentration of adsorbate, and burn-off of the activated carbons. The equilibria results obtained in a batch contactor were fitted by the Langmuir equation. The calculated values of ΔG demonstrate that the adsorption of the dye onto these activated carbons occurs by physical adsorption. Both the apparent values of ΔH and ΔS are positive, indicating that the adsorption process is endothermic and can produce spontaneously in our experimental conditions. The kinetic study was developed using a second-order exponential decay equation and the results were correlated using the Lagergren first-order equation relative to the concentration on the solid phase. The intraparticle diffusion coefficients have been estimated on the basis of an internal diffusion controlling mechanism for the net adsorption rate.

Keywords: Activated carbon, liquid phase application, adsorption equilibrium, adsorption kinetics, methylene blue

Received 10 December 2006, Accepted 28 May 2007
Address correspondence to L. M. Cotoruelo, Departamento de Ingeniería Química, Universidad de Málaga, Málaga 29071, España. Tel.: +34 952 13 20 37; Fax: +34 952 13 20 38; E-mail: lcot@uma.es

INTRODUCTION

Recent estimations indicate that approximately 12% of synthetic textile dyes used each year are lost during manufacture and processing operations, and 20% of these lost dyes enter the environment through effluents that result from the treatment of industrial wastewaters (1). The presence of colored wastewaters into the ecosystems is an important source of aesthetic pollution, and perturbation in the aquatic life as well, not only for their high chemical and biological oxygen demands, suspended solids, and content in toxic compounds but also for the color itself, which, being visible, is the first contaminant to be recognized (2).

Several properties of most dyes have been investigated and, in general, their tinctorial capacity is very high; less than 1 ppm of the dye produces obvious coloration. Conventional biological and chemical methods are not successful enough due to the non-biodegradable nature of most dyes. Although biological treatment processes effectively remove BOD, COD, and suspended solids, they are largely ineffective in removing color from wastewater. The advanced treatment methods for the removal of color and dyes include coagulation, chemical oxidation, and membrane separation processes (3). In addition, liquid-phase adsorption is actually one of the most efficient methods for the removal of colors, odors, and organic pollutants from process or waste effluents.

The application of the activated carbon as adsorbent is one of the most effective physical processes for the removal of color and the treatment of textile effluents (4–7). Many industrial and agricultural by-products such as bagasse, sawdust (8–10), corncobs, fruit stones, coconut, and nut shells have been used as a source for activated carbon (11, 12).

The remarkable adsorption properties of the activated carbons are due to their well-developed porous internal structure as well as the various surface functional groups. Activated carbons have been considered as amorphous carbons that show a very disordered microcrystalline structure in which graphitic micro-crystals are randomly oriented (13). The existing disorder among the graphitic layers due to the concentration of defects in the crystal involves the gaps between the micro crystals. Most of the pore structure is created during the activated carbon preparation. An adequate activation process leads to a maximum development of the pores and removes carbon atoms from the most reactive zones, hence enlarging the pores and/or increasing their number. The removal of carbon atoms, along the activation step, is not uniform due to the different crystalline grade of the carbon. This situation leads to surface heterogeneity involving a modification of the pore texture. However, the specific mechanism by which the adsorption of many compounds, especially organic compounds, takes place on this adsorbent, is still ambiguous. This is because the liquid-phase adsorption is a more complicated process than gas-phase adsorption (14). In addition, the mechanism of dye adsorption onto porous solids is rather complicated because of the

structure of the dye solution itself. This structure is usually discussed in terms of monomer-dimmer equilibrium although the presence of higher micelles or aggregates in concentrated solutions is also possible (15).

The physically and energetically heterogeneous nature of the solid surface, as it has been said, is a complicating factor. So, the available surface to the large dye molecules may contain, in the geometrical and energetic sense, a wide range of adsorption sites with different adsorptive power. This factor operates so far as to obscure the meaning of the isotherm that describes the adsorption, and complicates the thermodynamic analysis about the temperature dependence on the adsorption. Notwithstanding, adsorption isotherms are normally developed to evaluate the capacity of activated carbons for the adsorption of a particular molecule. They constitute the first experimental information, which is generally used to discriminate among different activated carbons and thereby to choose the most appropriate one for a particular liquid phase application. In this way, the literature indicates that the adsorption of phenol, methylene blue, caffeine, and iodine, among others, from the aqueous phase is a useful tool for monitoring the production and properties of activated carbons (15–19). In the present work, methylene blue has been used for this purpose; methylene blue (MB) is a thiazine (cationic) dye, widely used for dyeing cotton, wool, and silk. The main objective of this work was to determine the adsorption capacity of twenty powdered activated carbons prepared from eucalyptus kraft lignin, to remove MB from aqueous solutions, as a test for their possible application in liquid phase. The activation temperature and time are the main variables that influence the resulting burn-off of the prepared activated carbons. The experimental data were analyzed by employing the Langmuir equation for equilibria. Kinetic studies have been developed as well. We have used empirical models to arrange the adsorbate transfer between the liquid and the solid phases as the adsorbent surface is covered. Another objective was the estimation of the apparent diffusion coefficients for the intraparticle adsorption (20). Among activated carbons, we have analyzed and compared the adsorption capacities and rates in terms of their surface properties, mainly, specific surface area and pore distribution.

MATERIALS AND METHODS

Preparation of the Activated Carbons

The activated carbons have been prepared in our laboratory according to the procedure described in previous works (21, 22). Eucalyptus kraft lignin used as raw material in this work was supplied by the Empresa Nacional de Celulosas (ENCE, S.A.) as obtained by acid precipitation of kraft black liquors. The starting lignin has a high content in inorganic matter ($\sim$12% ash) so it has been previously treated by predevolatilization at low temperature

(623 K) under N_2 atmosphere. This temperature was reached at 10 K/min and maintained for 2 h. The resulting precarbonized was washed with 1% H_2SO_4 aqueous solution to lower its final ash content (less than 2% in all the cases).

This precarbonized substrate was used to obtain two carbonized at 823 K and 1073 K, respectively, which were used for the preparation of activated carbons (series A and B) as well as to obtain, directly, activated carbons (series C, D, and E). Carbonization and activation were carried out in a laboratory horizontal tubular furnace provided with temperature and heating rate controls. Certified 99.998% N_2 and CO_2 at 150 mL (STP)/min continuous flow were used in the carbonization and activation runs, respectively, and a 10 K/min heating rate was always used to reach the final temperature. Holding time at final temperature was set at 2 h for carbonization, and different times ranging, from 4 to 50 h, were used for activation to achieve a wide range of burn-off values. The activation temperature was studied by observing the surface porosity properties of the obtained activated carbons as well.

The porous structure of the ACs was characterized by means of adsorption-desorption of N_2 at 77 K and CO_2 at 273 K using a Quantachrome apparatus (Autosorb-1 model), and mercury porosimetry using a Carlo Erba mercury porosimeter 4000. All samples were degassed at 423 K under vacuum for 24 h, prior to the adsorption experiments. Particle densities (ρ_p) were determined from the mercury displacement method. Scanning electron microscopy (SEM) was applied to study the microstructure of the activated carbons. SEM micrographs were obtained by means of a model JSM 840 Jeol apparatus. The average sizes (radius) of the activated carbon particles were estimated using an image analysis procedure (A20: 4.48 μm; E12: 3.68 μm). In addition, tests carried out to determine the ACs pH values (ASTM D3838-80) showed no acid or base neutralizing capacity.

Adsorption Procedure

Methylene blue (MB), a cationic dye (CI. 52015), was supplied by Merck [$C_{16}H_{18}ClN_3S \times H_2O$ (x = 4–5)]. Its chemical structure is shown in Fig. 1; this molecule has a planar structure with the following dimensions: width 1.60 nm, depth 0.84 nm, and thickness 0.47 nm (23).

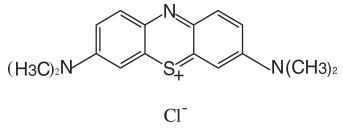

Figure 1. Chemical structure of methylene blue.

The adsorption equilibrium experiments were carried out using doses of 10.0 mg (dry basis) of activated carbon. Those were weighted and put into glass flasks. 100 mL of aqueous solutions of different initial MB concentrations (0.025–0.750 mmol/L) were added and mechanically agitated at 180 rpm using an orbital incubator (Gallenkamp, model INR-250). The samples were kept at different test temperatures until equilibrium were reached. This contact time varied between two and three weeks, time enough to reach the adsorption equilibrium. The temperatures for the different experiments varied in the range 278–313 K. MB equilibrium concentrations were determined by visible spectroscopy. An UV-Visible (Varian, model Cary 1E) spectrophotometer was used for the analysis. A calibration curve was prepared by recording the absorbance values for a range of known concentrations of dye solutions at the wavelength for maximum absorbance (λ_{max}: 664 nm). For the spectrophotometer used (path of light: 1 cm), the calibration equation ($r = 0.999$) were developed for the 0–2.5 mg/L range.

The effect of the pH on the amount of the removed dye was analyzed at the pH range from 2 to 12. pH values of initial concentrations were set using 0.1 N NaOH and 0.1 N HCl solutions. In this study 100 mL of dye solution of 0.250 mmol/L was shaken with 10.0 mg of activated carbon at 293 K. Samples without any activated carbon, showed no impact of pH change on the dye solutions. The pHs of the solutions were measured by using a micropH 2002 Crison pHmeter.

Equilibrium concentrations of retained MB on the adsorbent phase q_e (e.g. in mmol/g) were calculated by using the following equation:

$$q_e = \frac{C_o - C_e}{w} \tag{1}$$

where: C_o and C_e are the initial and the equilibrium concentrations of dye in solution (mmol/L), respectively and w is the adsorbent dose (g/L).

The adsorption kinetic experiments were carried out using a shaken batch of 500 mL capacity. MB solutions of 0.250 mmol/L were placed with doses of AC, and were agitated. All experiments were conducted at an agitation speed of 550 rpm. At certain intervals of time, the solution was analyzed, and the following equation was applied:

$$q_t = \frac{C_o - C_t}{w} \tag{2}$$

where: q_t (mmol/g) and C_t (mmol/L) are the concentration of MB on the adsorbent and in the liquid phase at time t (min), respectively. For the kinetic study ACs doses were 50, 100, and 150 mg/L. Tested temperatures were 293 K, 303 K, and 313 K. The maximum contact time was 3 hours.

RESULTS AND DISCUSSION

Activated Carbons

Five series of activated carbons were prepared (series A to E). Samples representing low, intermediate, and high activation degrees were prepared in each case. Table 1 summarizes the activation operating conditions, yield in AC (% weight) related to the initial lignin, and the overall burn-off (B.O. %) calculated as the sample weight loss relative to completely devolatilized kraft lignin. The designation of the samples makes uses of the activation time of each sample. It is found that the yield decreases with increasing time, and activation temperature under the conditions studied. Preliminary experiments showed that very high burn-offs were required to produce significant mesoporosity. This tendency has been reported in the preparation of the activated carbons from wood sawdust (9, 10) several agricultural wastes such as bamboo, plum kernels, corn cobs, and other sources such as the used automotive tires (24).

N_2 adsorption isotherms and mercury porosimetry have been developed for all of the samples; from these analysis we have calculated the total surface area (A_{BET}), external area (A_s), particle density (ρ_p), and the pore

Table 1. Operation conditions for the preparation of the different ACs series, burn-off (%), and yield (%)

AC	T.Carb. (°C)	T.Gasif. (°C)	t.activ. (h)	B.O. (%)	Rend. (%)
A4	550	800	4	27.5	31.6
A12	550	800	12	40.4	26.0
A20	550	800	20	51.4	21.2
A40	550	800	40	66.7	14.5
B4	800	800	4	8.10	36.2
B12	800	800	12	36.8	24.9
B20	800	800	20	54.8	17.8
B40	800	800	40	71.3	11.3
C20	350	750	20	26.2	29.4
C30	350	750	30	32.9	26.7
C40	350	750	40	49.9	20.1
C50	350	750	50	67.3	12.7
D4	350	800	4	11.5	33.4
D19	350	800	19	51.2	19.5
D30	350	800	30	65.8	14.5
D40	350	800	40	70.5	11.3
E4	350	850	4	21.3	31.5
E12	350	850	12	54.5	18.2
E16	350	850	16	63.5	13.9
E20	350	850	20	76.8	9.4

volume as micro, meso and macropore. The values of these results are summarized in Table 2. As can be observed, in all of the series, an important development of porosity takes place as activation proceeds. Surface area and micropore volume substantially increase with burn-off; widening of micropores, and increasing mesopores contribution are observed and, at high burn-off levels, a substantial development of macroporosity can be noticed. E20 has the highest surface area and total pore volume, and consequently, it is the least dense one.

SEM photographs of the activated carbons (Fig. 2) at different magnifications clearly reveal their surface texture and porosity, and they allow the identification a morphological class of particles, considered as rough spheres with many small holes on their surface.

Adsorption Equilibrium Isotherms

The adsorption experiments have been carried out to study the evolution of the MB concentration in the liquid phase until equilibrium values. Figure 3 shows the concentration decay curves at 293 K for MB adsorption on the ACs with

Table 2. Physical properties of ACs. A_{BET}: total specific surface area; A_S: external specific surface area; pore volumes; d_p: particle density

AC	A_{BET} (m^2/g)	A_S (m^2/g)	$V_{microp.N_2}$ (cm^3/g)	$V_{microp.CO_2}$ (cm^3/g)	V_{mesop} (cm^3/g)	V_{macrop} (cm^3/g)	V_{total} (cm^3/g)	ρ_p (g/cm^3)
A4	760	45.7	0.312	0.267	0.099	0.026	0.437	0.579
A12	926	130.3	0.384	0.307	0.236	0.044	0.664	0.483
A20	1049	254.0	0.413	0.326	0.398	0.081	0.892	0.417
A40	1450	724.5	0.528	0.380	0.992	0.510	2.030	0.230
B4	641	28.7	0.252	0.242	0.055	0.024	0.331	0.661
B12	888	158.5	0.356	0.287	0.291	0.041	0.688	0.467
B20	1123	354.4	0.426	0.354	0.714	0.189	1.329	0.318
B40	1343	509.9	0.567	0.366	0.740	0.343	1.650	0.270
C20	837	99.8	0.339	0.336	0.040	0.020	0.399	0.540
C30	947	108.0	0.389	0.349	0.170	0.040	0.599	0.490
C40	1211	261.5	0.473	0.355	0.270	0.070	0.813	0.398
C50	1319	372.9	0.510	0.372	0.490	0.240	1.240	0.276
D4	747	22.6	0.301	0.300	0.020	0.020	0.341	0.738
D19	1123	215.5	0.468	0.334	0.630	0.060	1.158	0.470
D30	1434	344.5	0.572	0.378	0.730	0.210	1.512	0.350
D40	1613	366.5	0.576	0.384	0.770	0.310	1.656	0.283
E4	822	36.1	0.331	0.304	0.060	0.020	0.411	0.630
E12	1273	341.3	0.483	0.339	0.480	0.110	1.073	0.441
E16	1348	393.0	0.531	0.351	0.780	0.150	1.461	0.307
E20	1853	504.2	0.701	0.376	0.860	0.530	2.091	0.240

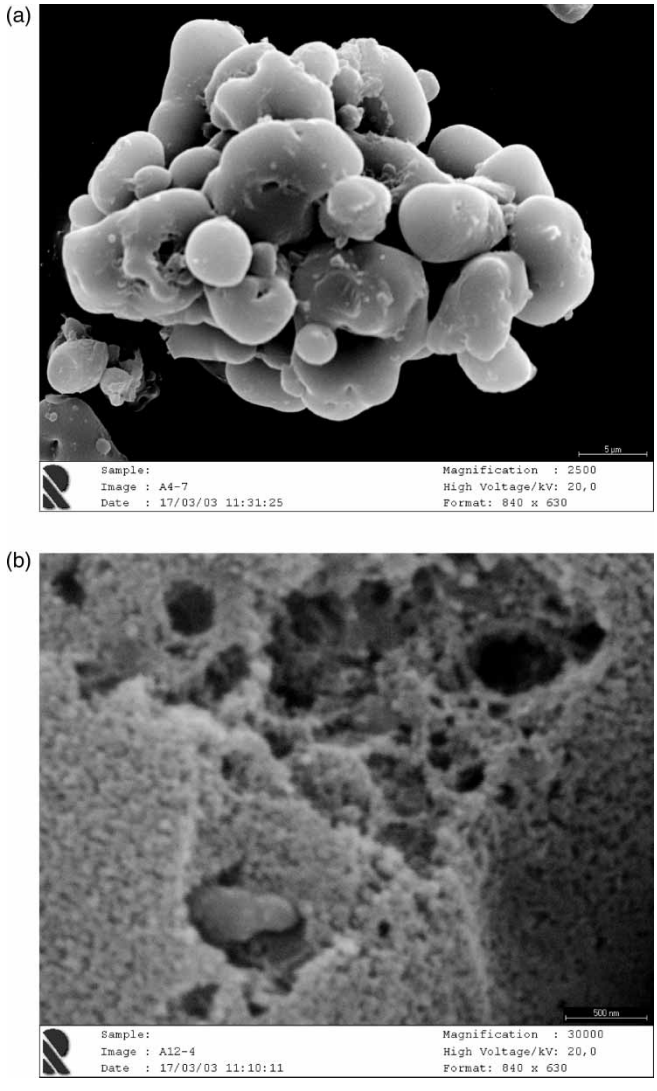

Figure 2. SEM of the external surface: a) A20 b) E12.

the highest B.O. of each series. The figure exhibits how the amount of MB in aqueous solution decreased with time. Preliminary investigations on the rate of MB adsorption on ACs indicated that the processes are quite rapid and, in most of the cases, about 70–80% of the ultimate adsorption can occur during the first hour of contact (adsorption on the mesopores). Subsequently adsorption continues very slowly, until equilibrium. The equilibrium is achieved in 15 days approximately. It is important to remember that the

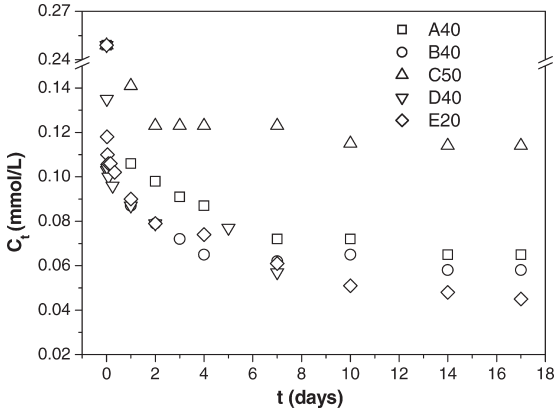

Figure 3. Curves for MB adsorption on A40, B40, C50, D40, and E20. C_o: 0.250 mmol/L; T: 293 K; pH: 6.8; w: 0.100 g/L.

high molecular weight and the maximum dimension of the MB molecule can cause difficulties to the molecules' migration through the adsorbent pores.

It can be observed that the time required to attain the equilibrium is the shortest for C50 that is characterized by the lowest developed pore volume. As can be seen in Table 2, the other adsorbents show higher mesopore volume values than C50. This explains, in part, their highest adsorption efficiency for the MB removal. This leads to the conclusion that mesopores act as transport conduits and largely contribute to the adsorption kinetics and equilibrium.

The adsorption isotherm is an expression for the variation of the adsorbent adsorption capacity with the concentration of adsorbate in the bulk solution at a constant temperature. Thus, adsorption isotherms are basically important to describe how the solutes interact with the adsorbents, which is fundamental in optimizing their use. The experimental isotherm is useful to quantify the adsorption capacity, i.e., for the selection of the most suitable adsorbent and for the preliminary determination of the adsorbent dosage requirements. Therefore, the isotherm plays an essential role in the predictive modelling procedure for analysis and design of adsorption systems. Figure 4 shows the MB adsorption isotherms of the twenty ACs used in this work at 293 K. The shape of the isotherms indicates a strong affinity of the dye towards the adsorbents. The isotherms can be classified within types H (high affinity of adsorbent for the solute at low concentrations) and L of the Giles adsorption isotherms classification (25). The L shape of the isotherms means that there is no strong competition between the solvent and the adsorbate to occupy the adsorbent surface sites. They are concaves with respect to the x-axis (concentrations in the fluid phase, C_e) and favorable to the activated carbon capacity to retain the adsorbate

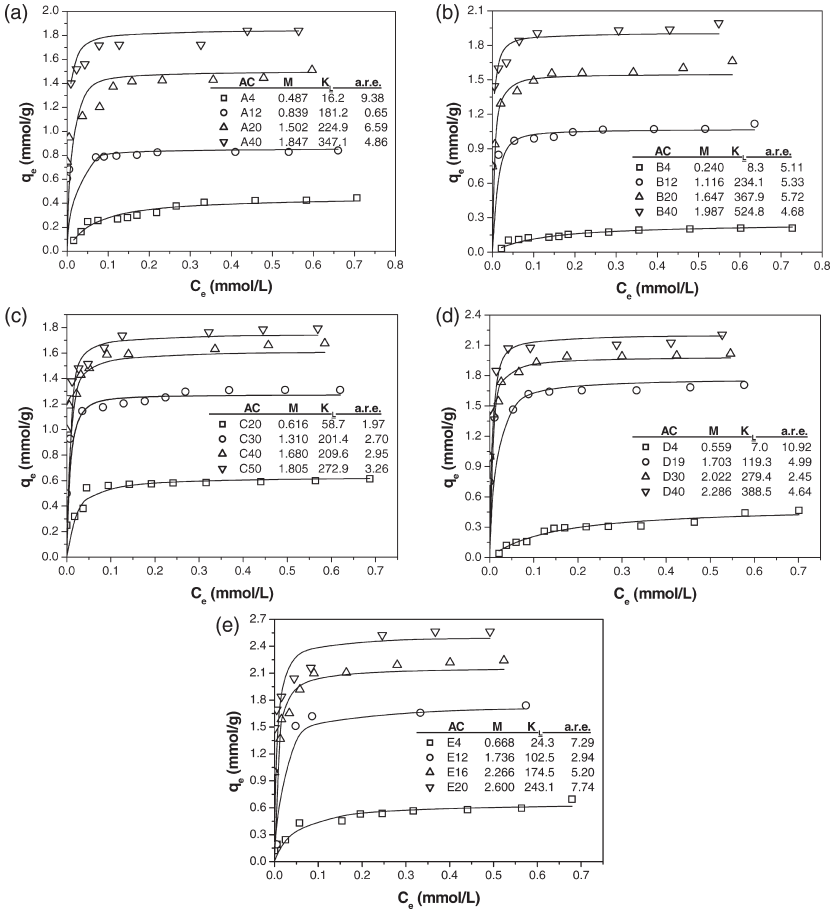

Figure 4. Experimental data (dots) and Langmuir fits (curves) for MB adsorption (293 K) isotherms on ACs series: a) A, b) B, c) C, d) D, and e) E.

at low concentrations. The adsorbed amount (in each series) rises with increasing the AC activation grade (Table 1). This increase in the adsorption capacity is a consequence of a greater surface area, as well as the mesoporosity development that take place when the activation grade is increased. A growth in mesoporosity (20–500 Å pore width), as an enlargement in microporosity, favour the adsorption rate and capacity.

According to the experimental data shown in Fig. 4, it is expected that the common two-parameter Langmuir equation can be applied:

$$q_e = \frac{K_L M\, C_e}{1 + K_L C_e} \tag{3}$$

where: K_L is the Langmuir equilibrium constant and M is the equilibrium concentration of adsorbate on the solid phase corresponding to a complete coverage (maximum adsorption capacity) of available adsorption sites.

To obtain the K_L and M values we have used the Langmuir isotherm as two linear forms:

$$\frac{C_e}{q_e} = \frac{1}{K_L M} + \frac{C_e}{M} \tag{4}$$

$$\frac{1}{q_e} = \frac{1}{M} + \frac{1}{K_L M\, C_e} \tag{5}$$

By using Eq. 4, M was calculated from the slope of the linear plot of C_e/q_e vs $C_e \cdot K_L$ was calculated from the slope of $1/q_e$ vs. $1/C_e$ plots (Eq. 5). Only values of the slopes of the straight lines have been used with the purpose of eluding possible errors associated to the extrapolations to the origin of coordinates. The Langmuir equation (curves) provides good prediction for high concentrations of solute matching with the experimental maximum adsorption but it yielded worse fits at low adsorbate concentrations.

The Langmuir constants (K_L in L/mmol; M in mmol/g) and the average relative error of the q_e predicted values (a.r.e. %) are summarized in the tables associated with Fig. 4. The M values can be transformed to the MB equivalent surface (A_{MB}) covering per gram of AC assuming that the MB molecules take a parallel orientation on the AC surface and the surface area covered by each adsorbed molecule is 1.344 nm^2 (23). It is of interest to have an idea about the grade of covering reached at the maximum adsorption conditions. Table 3 shows the values of the equivalent occupied area and the coverage factors for the MB adsorption.

At sight of the results, the equivalent coverage of the ACs surfaces by the MB molecules approach the BET specific surfaces. Nevertheless, the coverage factor for the most microporous ACs is rather lower due to the least available porosity. On the other hand, the activated carbons with high activation grade present a greater level of coverage by adsorption on the pores of intermediate size and also the possibility of constituting a multilayer in the adsorption as MB dimmers. An extension of the Langmuir equation was made by introducing a dimensionless equilibrium parameter, R_L (26), called the separation factor, given by:

$$R_L = \frac{1}{1 + K_L C_e} \tag{6}$$

where C_e is any liquid phase concentration of the adsorbate in equilibrium with the adsorbent. It is suggested that for favorable adsorption, $0 < R_L < 1$. Table 3 includes the separation factor for each AC, corresponding to the maximum experimental values of C_e in each isotherm (Co: 0.750 mmol/L).

The amount of MB adsorbed rose with the temperature increase, as can be seen in Fig. 5, indicating that the dye adsorption is favored at high temperatures.

Table 3. Equivalent specific surface of MB corresponding to M, coverage factor, and factor of separation (R_L)

AC	A_{MB} (m^2/g_{AC})	Cover. fact. A_{MB}/A_{BET}	R_L
A4	394.2	0.519	0.080
A12	679.2	0.733	0.008
A20	1215.9	1.159	0.007
A40	1495.1	1.031	0.005
B4	194.3	0.303	0.142
B12	903.4	1.017	0.006
B20	1333.2	1.187	0.004
B40	1608.5	1.198	0.003
C20	498.6	0.596	0.024
C30	1060.4	1.120	0.008
C40	1360.0	1.123	0.008
C50	1461.1	1.107	0.006
D4	452.5	0.606	0.169
D19	1378.6	1.228	0.014
D30	1636.8	1.141	0.006
D40	1850.5	1.147	0.004
E4	540.7	0.658	0.057
E12	1405.3	1.104	0.016
E16	1834.3	1.361	0.010
E20	2104.7	1.136	0.008

This suggests the endothermic nature of the entire process. In order to explain this increase of the adsorption when the temperature is increased, it is necessary to consider the variation in the aggregating state that MB molecule can present in aqueous dissolution. MB cation in dissolution is mainly in the monomer and the dimmer forms, although it can also present higher aggregation forms according to its concentration (27). The MB molecule presents a greater facility to adsorb as a monomer (due to the size effects), whereas the aggregation increase leads to a high difficulty to penetrate into micropores and narrow mesopores. An increase of temperature favors the dimmers dissociation, which is of endothermic character. The proportion of monomers is more abundant at high temperatures than at low. The micelles or ionic aggregates of the dye are prevalent at low temperatures (15).

Thermodynamic Study

A better knowledge of the phenomena implied during the adsorption of a particular molecule on activated carbons is obtained by a thermodynamic approach to the adsorption mechanism. The thermodynamic analysis

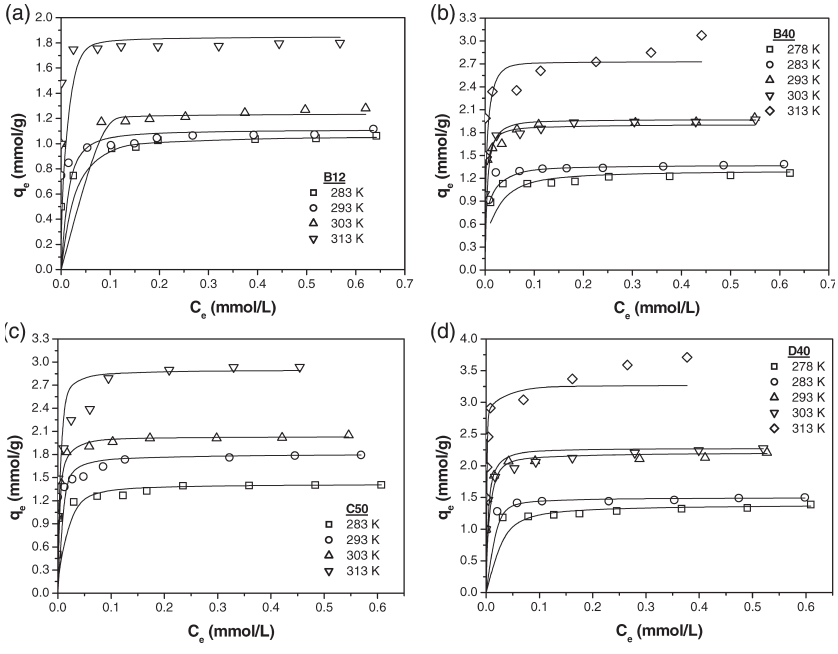

Figure 5. Experimental data (dots) and Langmuir fits (curves) for MB adsorption isotherms on ACs at different temperatures: a) B12, b) B40, c) C50, and d) D40.

provides information about the process ability to take place and the stability of the adsorbed phase as well. The changes on the free energy, enthalpy, and entropy of the adsorption processes of MB on ACs in a range of temperature between 278 K and 313 K were calculated using the following equations:

$$\Delta G = -RT \text{ Ln } K_L \tag{7}$$

$$\frac{\partial \text{Ln } K_L}{\partial T} = \frac{\Delta H}{RT^2} \qquad \text{Integrating} \tag{8}$$

$$\text{Ln } K_L = \text{Ln } K_o - \frac{\Delta H}{RT} \tag{9}$$

$$\Delta S = \frac{\Delta H - \Delta G}{T} \tag{10}$$

where: R is the gases constant, T is the absolute temperature, and K_o is a frequency factor. Once the Langmuir constant (K_L) is determined; the dependency of the adsorption process with the temperature can be studied. The values of the Langmuir equation parameters for the MB adsorption at different temperatures and the values of ΔG, ΔH, and ΔS obtained are given in Table 4 for a selection of representative activated carbons (B12, B40, C50, and D40).

Table 4. Values of Langmuir equation fits and thermodynamic values in MB adsorption. ΔH (kJ/mol); ΔG (kJ/mol); ΔS (J/mol K); K_o (L/mmol); K_L (L/mmol); M (mmol/g)

		278 K	283 K	293 K	303 K	313 K
B12	ΔG	n.a.	−10.62	−13.28	−15.04	−16.41
ΔH:43.48	ΔS	n.a.	191.2	193.7	193.2	191.3
K_o: 1.1 E10	K_L	n.a.	91.8	234.1	394.6	550.9
	M	n.a.	1.067	1.116	1.281	1.797
B40	ΔG	−10.14	−12.57	−15.24	−16.34	−18.81
ΔH:53.96	ΔS	230.6	235.1	236.2	232.0	232.50
K_o: 1.5 E12	K_L	80.7	210.0	524.8	661.7	1388.0
	M	1.276	1.389	1.987	1.973	3.040
C50	ΔG	n.a.	−11.98	−13.65	−15.99	−17.67
ΔH:42.94	ΔS	n.a.	194.0	193.1	194.5	193.6
K_o: 1.4 E10	K_L	n.a.	163.2	272.9	573.9	894.6
	M	n.a.	1.418	1.805	2.033	2.973
D40	ΔG	−10.04	−13.32	−14.51	−15.70	−18.88
ΔH:49.63	ΔS	214.6	222.4	218.9	215.6	218.9
K_o: 2.5 E11	K_L	77.5	288.8	388.5	511.4	1425.4
	M	1.383	1.501	2.286	2.279	3.673

Equation 7 relates the Gibbs free energy change of the adsorption process with the equilibrium constant. The negative values of ΔG (Table 4) indicate the feasibility of the process and the spontaneous nature of MB adsorption on the adsorbents. The solute is expected to be more concentrated on the surface of the activated carbon than in the bulk solution. Absolute ΔG values increase as temperature increases, indicating that the entire process is favoured at the highest temperatures.

The enthalpy of adsorption (isosteric heat) is given by the van't Hoff equation Eq. (9) (28, 29). If ΔH is constant at the interval of studied temperatures, experimental data will be on a straight line by plotting Ln K_L vs. 1/T. For example, the ΔH values for B12 and C50 were calculated from the slopes of the lines in Fig. 6. Positive values of ΔH (Table 4) confirm the endothermic nature of the overall process. As has been said, this is because of the endothermic dissociation of the dimmers, micelles, or ionic aggregates of the dye. The monomers (rather abundant at high temperatures) can adsorb within the micropores, and are less accessible to the molecular aggregates of the solute. So, despite the exothermic nature of the physical adsorption step itself, the apparent enthalpy change of the process becomes positive.

The entropy changes associated with the adsorption processes can be calculated from the Gibbs-Helmholtz equation (Eq. 10). The positive values of ΔS (Table 4) show a gain in the molecular disorder after the adsorption of MB occurs. Increases in entropy were reported, e.g., in systems of diazinon/activated sludge (29) as well as for the adsorption of aromatic

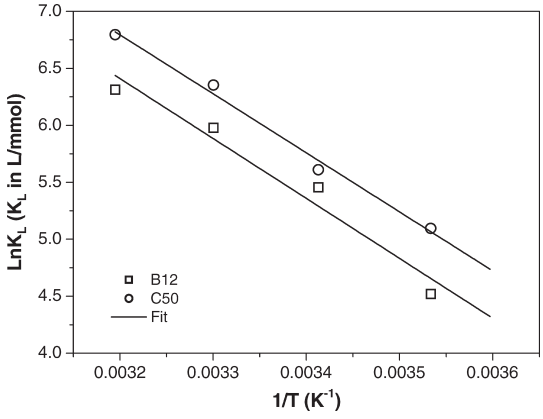

Figure 6. Adsorption enthalpy estimations for MB adsorption on B12, and C50.

carboxylic acids on carbon blacks (30). They concluded that for large molecules, the simplified view of the more ordered arrangement of molecules on the surface may not be appropriate, and that non specific interaction energy between the adsorbate and the surface—coupled with configurational changes in the adsorbate on adsorption—could account for the positive entropy changes. Negative values of ΔG and positive for ΔH and ΔS also have been found in the adsorption of malachite green from wastewater using activated carbon and activated slag (3).

Nevertheless, it is necessary to remind that ΔG, ΔH, and ΔS calculated values represent the apparent behaviors associated with the studied adsorption processes at the interval of temperatures and the other experimental conditions.

Effect of pH on Adsorption

Most of dyes are ionic chemicals that dissociate in aqueous solution. The degree of adsorption of these ionized forms on the adsorbent surface is primarily influenced by the charge on the adsorbent surface, which is influenced by the solution pH (31). Activated carbon materials act with the amphoteric character. Depending on the pH of the solution, their surfaces may be positively or negatively charged. At $pH > pH_{PZC}$ the activated carbon surface becomes negatively charged favoring the adsorption of the cationic species. This is the case of the cationic MB that can be expected to have the greatest affinity to the AC surface at the highest pH. On the other hand, the adsorption of anionic species will be favoured at $pH < pH_{PZC}$ (32).

A number of MB adsorption equilibrium experiments were carried out to study the pH effect on the MB adsorption onto B40, D40, and E20. A potential

model has been used to fit the experimental data.

$$q_e = a\,(pH)^b \tag{11}$$

where a and b are calculated constants (B40: $a = 0.713$, $b = 0.499$; D40: $a = 0.979$, $b = 0.364$; E20: $a = 0.991$, $b = 0.394$). Experimental data and potential model fits are plotted in Fig. 7. It was observed that the solution pH affects the amount of the adsorbed dye. Several reasons may be attributed to the dye sorption behavior related to solution pH. The low adsorption of MB at acid pH is probably due to the presence of high concentration of H^+ ions competing with the dye cationic groups for the adsorption sites. As the surface charge density increases with an increase in the solution pH, the electrostatic attraction between the positively charged MB cation and the surface of the activated carbon is enhanced, which may result in an increase in the adsorption capacity. Similar trends have been reported in the literature about the adsorption of MB on rice husk (12) and malachite green on agro-industry wastes (33).

The equivalent surface of the adsorbed MB molecules per gram of AC was calculated (Table 5) at two different pH values (3 and 10) considering the MB molecule cross-sectional area is 1.344 nm^2 (1.6 nm $\times$0.84 nm). At the lowest pH of the solution, the MB coverages were lower than the AC BET surface areas, but, in all of the samples at the highest pH, these surface coverages were greater than the BET surface areas, indicating that a multilayer adsorption occurred. The calculated values of coverage factors almost become multiplied by 1.5 as the pH was increased, depending on the considered AC.

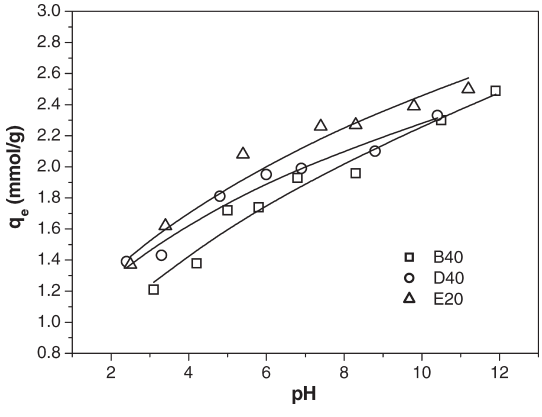

Figure 7. pH effect on the equilibrium of MB on B40, D40, and E20. Experimental data (dots) and potential model fits (curves). C_o: 0.250 mmol/L; w: 0.100 g/L; T: 293 K.

Table 5. Apparent specific area values occupied by MB, and coverage factor. q_e values from the potential model. C_o: 0.250 mmol/L; w: 0.100 g/L; T: 293 K

AC	pH	q_e (mmol $_{MB}/g_{AC}$)	A_{MB} (m^2/g_{AC})	Cov. fac. A_{MB}/A_{BET}
B40	3	1.233	998.10	0.743
D40	3	1.460	1182.7	0.733
E20	3	1.528	1236.9	0.667
B40	10	2.250	1821.4	1.356
D40	10	2.264	1832.7	1.136
E20	10	2.455	1987.3	1.072

As a complementary study, kinetic data have been obtained for MB on D30 adsorption at different pH values in the 1.9–11.3 range, which are presented in Fig. 8. It can be observed in this figure how as pH increases, MB adsorption rate and capacity increase as well. This can be explained because of the enhancement of the net negative charge on the AC surface at high pH values. As has been said, this environment favors a high affinity between the AC surface and the MB cationic structure, strong attraction forces occur, which lead to a high adsorption rate. Nevertheless, it may not be practical to maintain extreme pH values because it would need the addition of chemicals to raise the pH and the effluent would need a neutralization final step before discharge.

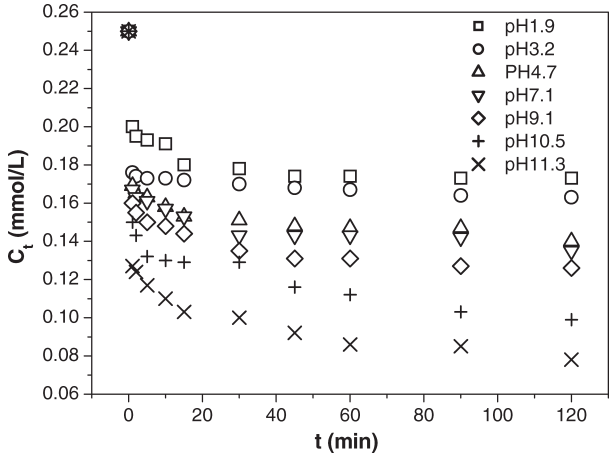

Figure 8. Kinetic of MB adsorption on D30 at different pH. C_o: 0.250 mmol/L; w: 0.100 g/L; T: 293 K.

Comparison Among Activated Carbons

Figure 9 shows the maximum adsorption capacity (M) of MB vs. burn-off for all the studied activated carbons. A lineal trend has been obtained from this plot, with $r^2 = 0.952$. The favorable effect of the activation degree (in each series) on the adsorption capacity can be confirmed. B4 has a very low capacity (0.240 mmol/g) while E20 shows a very high capacity (2.600 mmol/g). The others show intermediate adsorption capacities. This is in agreement with their internal surface area development and more especially with the volume of mesopores.

In the gasification process, an increase in activation time and temperature leads to a high developed surface area, and a high burn-off and adsorption capacity as well. The best results correspond to E20 active carbon.

Kinetic Study

The adsorption rate is governed by several factors such as the nature of the solute and the adsorbent, the pH, the AC dose, and the temperature of the medium. Knowing the influence of the operational parameters on the adsorption rate is the first step toward the understanding and control the process. In general, solid-liquid adsorption processes on porous materials may be described as a series of steps: external mass transfer from the liquid phase to the solid particle surface across the boundary layer, internal diffusion within the porous particle, and adsorption on the surface. The kinetic experiments were carried out using all the ACs. However, for the present study, as examples, the results from A20 and E12 were selected on the basis of their surface properties and adsorptive behaviours.

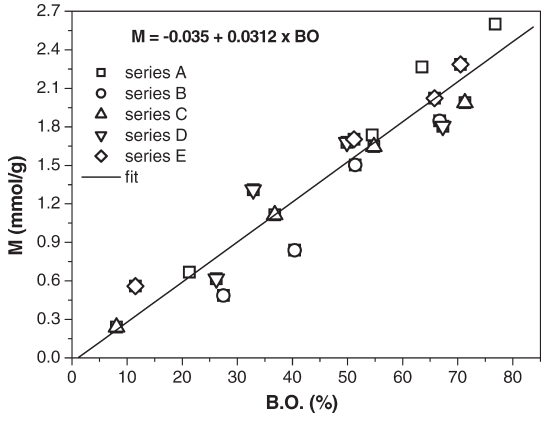

Figure 9. MB adsorption on ACs at 293 K. C_o: 0.750 mmol/L; w: 0.100 g/L.

The effect of the agitation on the extent of the adsorption was investigated by varying the agitation speed from 400 to 700 rpm under the selected agitation time and initial solute concentration (0.250 mmol/L). The shape of all the adsorption curves was similar with no variation in the extent of adsorption.

The removal of MB was studied at 293 K, 303 K and 313 K. Figure 10 plots the results for A20. The yield and rate of the adsorption of the dye at non-equilibrium contact times increase with temperature, indicating the activating effect of this variable. This may be a result of the increase in the mobility of the MB molecules as well as an improvement of the mass transfer parameters. Also, as mentioned earlier, the aggregation state of MB molecule decreases as temperature increases.

An empirical model was used for the adsorbate concentration decay in the aqueous phase. The experimental results for the MB adsorption at different doses and temperatures were fitted to the following second order exponential decay equation:

$$C_t = y_o + A_1\, e^{(-B_1 t)} + A_2\, e^{(-B_2 t)} \tag{12}$$

$$\frac{dq_t}{dt} = \frac{A_1\, B_1}{w} e^{(-B_1 t)} + \frac{A_2 B_2}{w} e^{(-B_2 t)} \tag{13}$$

where: y_o, A_1, B_1, A_2, and B_2 are empirical coefficients. As examples, the calculated coefficients are shown in Table 6 for A20 and E12. It includes the χ^2 (average quadratic deviation) values. Examples of the model (lines) are shown in Fig. 10. Because of $A_1 \sim 2A_2$ and $B_1 >> B_2$, it is appreciable that the first exponential term as written in Eq. (12) contributes to a good fit at very short time values (really for $t < 1$ min; $C_t \to y_o + A_1 + A_2$). At intermediate and high time values this first term becomes negligible and the good fit is

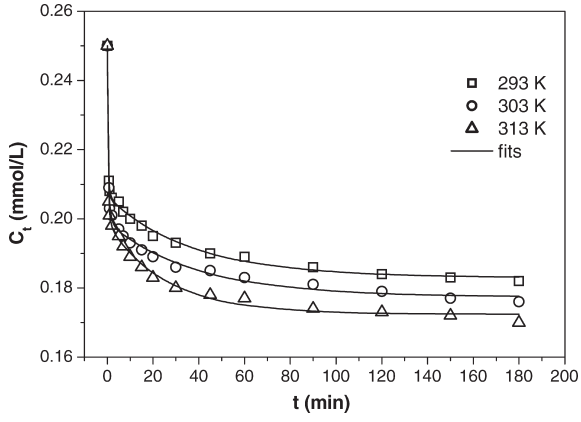

Figure 10. Temperature effect on the rate of MB adsorption on A20. C_o: 0.250 mmol/L; w. 0.100 g/L. Experimental data (dots) and fits (curves).

Table 6. Exponential decay coefficients for MB adsorption on A20, and E12. C_o: 0.250 mmol/L

	W: 0.050 g/L			w: 0.100 g/L			w: 0.150 g/L		
T(K)	293	303	313	293	303	313	293	303	313
MB on A20									
y_o	0.214	0.208	0.204	0.183	0.179	0.173	0.155	0.148	0.140
A_1	0.024	0.025	0.025	0.043	0.048	0.048	0.057	0.064	0.067
B_1	3.294	2.039	2.915	2.856	2.516	3.045	2.016	1.685	2.466
A_2	0.012	0.016	0.020	0.024	0.022	0.027	0.036	0.036	0.042
B_2	0.032	0.038	0.051	0.027	0.043	0.052	0.029	0.042	0.054
χ^2	1E-6	2E-6	9E-7	9E-7	3E-6	2E-6	6E-6	4E-6	3E-6
MB on E12									
y_o	0.204	0.202	0.198	0.163	0.162	0.152	0.127	0.123	0.112
A_1	0.029	0.034	0.036	0.057	0.063	0.057	0.077	0.082	0.083
B_1	2.995	1.836	3.538	2.987	2.042	3.600	2.063	2.260	3.670
A_2	0.016	0.014	0.015	0.030	0.024	0.040	0.045	0.044	0.054
B_2	0.047	0.066	0.086	0.049	0.065	0.085	0.049	0.063	0.086
χ^2	1E-6	4E-6	3E-6	5E-6	9E-6	1E-5	2E-5	2E-5	3E-5

reached due to the second exponential term contribution (i.e.: $C_t \approx y_o + A_2 \exp(-B_2 t)$). At very high contact times: $C_t \to y_o$.

Figure 11 shows the values of the adsorption rates referred to the MB concentration on A20 and E12 at 293 K. The data were provided using Eq. 13. A sharp decrease in the adsorption rate is observed for the first minutes of the contact time. This step corresponds to the fast surface coverage in the widest pores and the most active sites. A second step develops for one hour

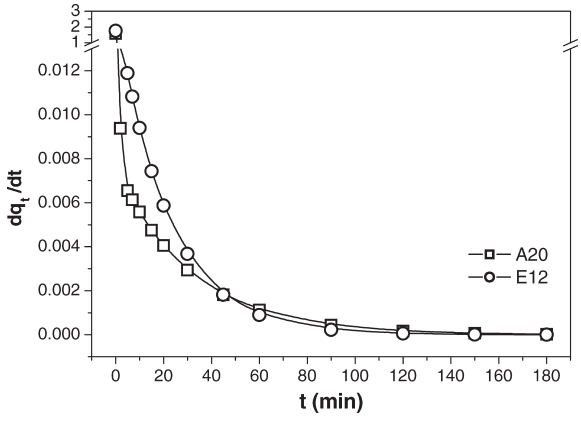

Figure 11. Adsorption rate decay curves. C_o: 0.250 mmol/L; T: 293 K; w: 0.050 g/L.

approximately with an intermediate decreasing rate. This step is the most interesting in order to get the kinetic control by its relation to the narrow mesopores and micropores coverage. The last part ends at the equilibrium conditions, after several days of contact time.

The rate for the increase of the adsorbate concentration on the solid phase was analyzed with success by using the pseudo-first order equation, first proposed by Lagergren (34), and later used by numerous authors (12, 35, 36). The pseudo-first order differential equation can be generalized for order n as follows:

$$\frac{dq_t}{dt} = k\,(q_m - q_t)^n \tag{14}$$

where k is the adsorption rate constant, n is the apparent order of the process related to the available adsorbent concentration $(q_m - q_t)$, which is the driving force of the process, and represents the vacant and accessible active sites in the surface of the adsorbent, for any time of contact t and q_m (mmol/g) is the maximum achievable coverage. Applying logarithms to Eq. (14) it becomes:

$$\log\left(\frac{dq_t}{dt}\right) = \log k + n\ \log\,(q_m - q_t) \tag{15}$$

The values of q_m can be calculated from Eq. (16) derived from Eq. (12) for $t = \infty$.

$$q_m = \frac{C_o - y_o}{w} \tag{16}$$

As an example, Fig. 12 shows (dq_t/dt) vs. $(q_m - q_t)$ for MB on A20 and E12 at 293 K. The values of k and n can be obtained from the intercept and

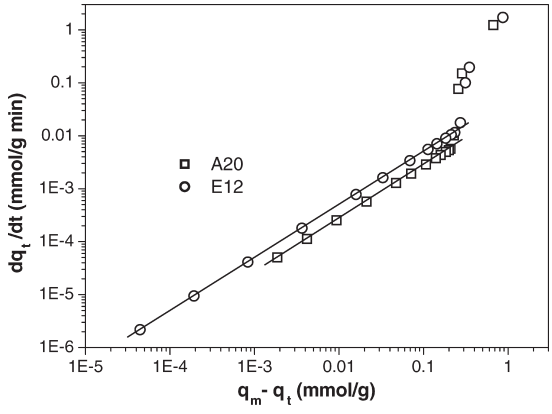

Figure 12. Kinetic order plots for MB adsorption on A20 and E12. C_o: 0.250 mmol/L; T: 293 K; w: 0.100 g/L.

the slope of the straight lines in the plots. The values of n were in all the cases very close to unity and the coefficients of linear regression were higher than 0.999, which verifies the applicability of this kinetic equation with an apparent first-order for the adsorption process of MB onto ACs. Nevertheless, it is observed that the slope in the first minutes is very high (high $(q_m - q_t)$ values), which means this corresponds to a very high initial adsorption rate that is strongly dependent on the high initial concentration of the available active sites. The values of k (min^{-1}) were: 0.029, 0.041, and 0.052 for A20 at 293 K, 303 K, and 313 K, respectively; and 0.048, 0.065, and 0.086 in the case of E12. The adsorption rate constants generally increase with temperature and the related apparent activation energies (E_a in kJ/mol) were also estimated according to an Arrhenius type equation:

$$k = k_A \exp\left(\frac{-E_a}{RT}\right) \tag{17}$$

where k_A (min^{-1}) is a frequency or preexponential factor. Ea values were calculated from the slopes of the Ln k vs. 1/T plots. Linear regression coefficients were 0.996 for A20, and 0.999 for E12. The magnitudes of E_a were: 22.2 kJ/mol (A20), and 21.8 kJ/mol (E12). The low values of E_a suggest a low influence of the temperature in the adsorption rate if is compared with that related to the available active sites.

Estimation of the Effective Diffusion Coefficients

The adsorbate transfer from the bulk of the fluid phase toward the active sites on the adsorbent internal surface previous to the adsorption step includes two main resistances: external diffusion within the boundary layer and internal diffusion into the porous particle (13). As said in the previous discussion the effect of shaking on the kinetics and adsorption capacity is negligible in this work, implying that the rate of adsorption in the porous adsorbent is rather controlled by the mass transfer into the pore network.

Adsorbent particles become heterogeneous systems formed by a porous solid phase and a fluid phase filling the void fraction of the solid. A number of models have been postulated, which differ in their description of the diffusion process into the pores (37). Intraparticle diffusion depends on many factors such as the structure of the adsorbent, the physical properties of the adsorbent and adsorbate, the chemical properties of the adsorbate, the equilibrium state, and the system conditions. Crank (38) developed the following equation for spherical particles:

$$\frac{q_t}{q_e} = 1 - \frac{6}{\pi^2}\sum_{n=1}^{\infty}\frac{1}{n^2}\exp\left(\frac{-D_S n^2 \pi^2 t}{R_P^2}\right) \tag{18}$$

where: R_P is the particle radius, D_S is the surface diffusion coefficient, that becomes an effective diffusivity (D_i) if we consider that the surface diffusion dominates the transport. In this case, the adsorbate molecules in the bulk phase surrounding the particle will locally equilibrate with the adsorbed molecules at the entrance of the pore, and so, the adsorbed molecules diffuse into the particle. In the literature it is found that short time solutions are needed to study the behavior of adsorption during the initial stage. For linear isotherms, this can be analytically achieved by taking Laplace transform of the model equation (39). So, for short times, or, more precisely, for $q_t/q_e < 0.3$, Eq. (18) becomes:

$$D_i = \left(\frac{q_t}{q_e}\right)^2 \frac{\pi R_P^2}{36\ t} \tag{19}$$

If the adsorption isotherm is not linear, the linear model is also satisfactory for adsorbates that are not very strongly adsorbed, and that show adsorption isotherms with smooth and moderate change of slope (40). Nevertheless, apparent diffusion coefficients generally vary with the surface concentration. For this study, we have calculated the effective diffusion coefficients from the kinetic results by using Eq. (19). The q_t values corresponding to different times were estimated by the exponential decay model Eq. (12). The q_e values were previously determined from the equilibrium experiments.

The continuous decrease of D_i values as the contact time increases is due to the consumption of the high energy adsorption sites and the spatial difficulties enhancement (examples in Figs 13 and 14). Those lead to a drop of the driving forces. This is especially notorious when, at advanced contact times, the adsorption on macro and mesopores is very slow and the adsorbate net

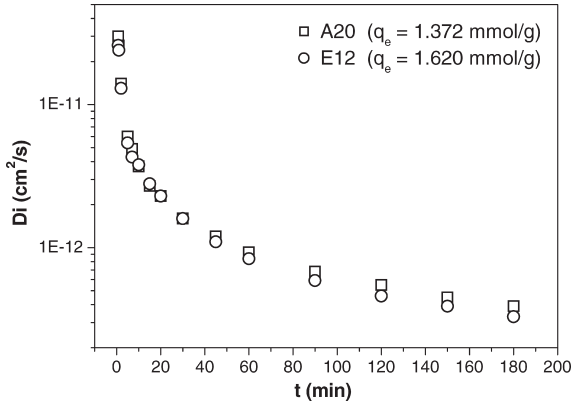

Figure 13. Effective diffusion coefficients for MB adsorption. Variation with time. C_o: 0.250 mmol/L; T: 293 K; w: 0.100 g/L.

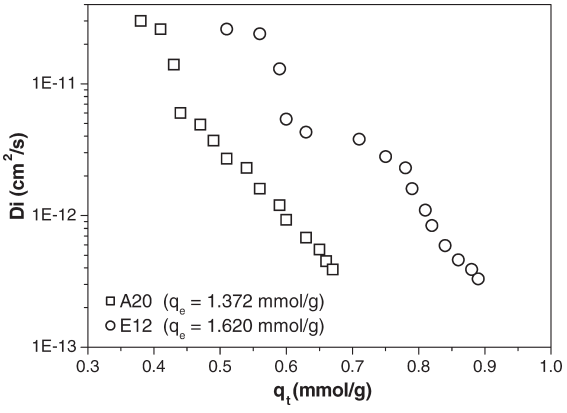

Figure 14. Effective diffusion coefficients for MB adsorption. Variation with the load on the adsorbents. C_o: 0.250 mmol/L; T: 293 K; w: 0.100 g/L.

flow (MB monomers and dimmers) within micropores becomes difficult because of the tortuosity, as well as the obstruction in the entrance to the pores.

CONCLUSIONS

Activated carbons obtained from lignin, at different experimental conditions, have been successfully employed as adsorbents for quantitative removal of MB from aqueous solution. The equilibrium data were fitted to the Langmuir isotherm and the maximum adsorption capacities were obtained for all the activated carbons. It has been found that the activated carbons burn-off influences on the adsorption capacity for all the activated carbon series. The thermodynamic analysis indicated that the MB adsorption was spontaneous and endothermic. The kinetic analysis revealed adsorption rates with linear dependence on the available active sites on the activated carbons surfaces.

ACKNOWLEDGMENT

The authors acknowledge the Spanish DGICYT (Project PPQ-2003/07160) and the Junta de Andalucía (PAI-TEP184) for the financial support.

REFERENCES

1. Voudrias, E., Fytianos, K., and Bozani, E. (2002) Sorption-desorption isotherms of dyes from aqueous solutions and wastewaters with different sorbent materials. *Global Nest: The Int. J.*, 4: 75–83.

2. Correia, V.M., Stephenson, T., and Judd, S.J. (1994) Characterization of textile wastewaters; A Review. *Environ. Technol.*, 15: 917–99.
3. Gupta, V.K., Srivastava, S.K., and Mohan, D. (1997) Equilibrium uptake, sorption dynamics, process optimization and column operations for the removal and recovery of malachite green from wastewater using activated carbon and activated slag. *Ind. Eng. Chem. Res.*, 36: 2207–2218.
4. Morais, L.C., Freitas, O.M., Gonçalves, E.P., Vasconcelos, L.T., and González Beça, C.G. (1999) Reactive dyes removal from wastewaters by adsorption on eucalyptus bark: variables that define the process. *Water Res.*, 33: 979–988.
5. Abu-El-Shár, W.Y., Gharaibeh, S.H., and Mahmoud, S. (2000) Removal of dyes from aqueous solutions using low-cost sorbents made of solid residues from olive-mill wastes (JEFT) and solid residues from refined Jordanian oil shale. *Environ. Geology*, 39: 1090–1094.
6. Costas, P. and Snoeyink, V.L. (2000) Competitive adsorption between atrazine and methylene blue on activated carbon: The importance of pore size distribution. *Carbon*, 38: 1423–1436.
7. Otero, M., Rozada, F., Calvo, L.F., García, A.I., and Morán, A. (2003) Kinetic and equilibrium modelling of the methylene blue removal from solution by adsorbent materials produced from sewage sludge. *Biochemical Engineering Journal*, 15: 59–68.
8. Tancredi, N., Cordero, T., Rodríguez-Mirasol, J., and Rodríguez, J.J. (1996) Activated carbons from uruguayan eucalyptus wood. *Fuel*, 75 (15): 1701–1706.
9. Tancredi, N., Cordero, T., Rodríguez-Mirasol, J., and Rodríguez, J.J. (1997) Activated carbons from eucalyptus wood. Influence of carbonization temperature. *Sep. Sci. Technol.*, 32 (6): 1115–1126.
10. Márquez-Montesino, F., Cordero, T., Rodríguez-Mirasol, J., and Rodríguez, J.J. (2001) Powdered activated carbon from pinus caribaea sawdust. *Sep. Sci. Technol.*, 36 (14): 3191–3206.
11. Bacaoui, A., Yaacoubi, A., Dahbi, C., Bennouna, J.A., and Mazet, M. (1998) Activated carbon production from moroccan olive wastes-influence of some factors. *Environ. Technol.*, 19: 1203.
12. Vadivelan, V. and Kumar, K.V. (2005) Equilibrium, kinetics, mechanism and process design for the sorption of methylene blue onto rice husk. *J. Colloid Interface Sci.*, 286: 90–100.
13. Noll, K.E., Gounaris, V., and Hou, W. (1992) *Adsorption Technology for Air and Water Pollution Control*; Lewis Pub. Inc.: Chelsea, Michigan.
14. Moreno-Castilla, C., Rivera-Utrilla, J., López-Ramón, M.V., and Carrasco-Marín, F. (1995) Adsorption of some substituted phenols on activated carbons from a bituminous coal. *Carbon*, 33: 845–851.
15. Barton, S.S. (1987) The adsorption of methylene blue by activated carbon. *Carbon*, 25: 343–350.
16. Avom, J., Mbadcam, J.K., Noubactep, C., and Germain, P. (1997) Adsorption of methylene blue from an aqueous solution on to activated carbons from palm-tree cobs. *Carbon*, 35: 365–369.
17. Zou, Y. and Han, B-X. (2001) Preparation of activated carbons from chinese coal and hydrolysis lignin. *Adsorp. Sci. Technol.*, 19: 59–72.
18. Zou, Y. and Han, B-X. (2001) High-surface-area activated carbons from chinese coal. *Energy and Fuels*, 15: 1383–1386.
19. González-Serrano, E., Cordero, T., Rodríguez-Mirasol, J., Cotoruelo, L., and Rodríguez, J.J. (2004) Removal of water pollutants with activated carbons

prepared from H_3PO_4 activation of lignin from kraft black liquors. *Water Res.*, 38: 3043.
20. Cotoruelo, L.M., Marqués, M.D., Rodríguez-Mirasol, J., Cordero, T., and Rodríguez, J.J. (2007) Adsorption of aromatic compounds on activated carbons from lignin: kinetic study. *Ind. Eng. Chem. Res.*, 46: 2853–2860.
21. Rodríguez-Mirasol, J., Cordero, T., and Rodríguez, J.J. (1993) Preparation and characterization of activated carbon from eucalyptus kraft lignin. *Carbon*, 31: 87–95.
22. Rodríguez-Mirasol, J., Cordero, T., and Rodríguez, J.J. (1993) Activated carbons from CO_2 partial gasification of eucalyptus kraft lignin. *Energy fuels*, 7: 133–138.
23. Kasaoka, S., Sakata, Y., Tanaka, E., and Naitoh, R. (1989) Design of molecular-sieve carbon. Studies on the adsorption of various dyes in the liquid phase. *Intern. Chem. Eng.*, 29: 734–742.
24. Juang, R.S., Tseng, R.L., Wu, F.C., and Lee, S.H. (1997) Adsorption behavior of reactive dyes from aqueous solutions on chitosan. *J. Chem. Tech. Biotechnol.*, 70: 391–399.
25. Giles, C.H., MacEwan, T.H., Nakhwa, S.N., and Smith, D. (1960) Studies in adsorption. part XI. A system of classification of solution adsorption isotherms, and its use in diagnosis of adsorption mechanisms and in measurement of specific surface areas of solids. *J. Chem. Soc.*, : 3973.
26. Hall, K.R., Eagleton, L.C., Acrivos, A., and Vermeulen, T. (1966) Pore and solid diffusion kinetics in fixed bed adsorption under constant pattern conditions. *Ind. Engng. Chem. Fund.*, 5: 212–219.
27. González Martín, M.L., Valenzuela Calahorro, C., and Gómez Serrano, V. (1991) Adsorción de p-nitrofenol en disolución acuosa por negros de carbón. Efecto de la temperatura. Entalpía de adsorción. *An. Quím.*, 87: 1036–1045.
28. Gustafson, R.L., Albright, R.L., Heisler, J., Lirio, J.A., and Reid, O.T. (1968) Adsorption of organic species by high surface area styrene-divinylbenzene copolymers. *I&EC Prod. Res. Dev.*, 7: 107–115.
29. Bell, J.P. and Tsezos, M. (1987) Removal of hazardous organic pollutants by biomass adsorption. *J. Water Pollut. Control Fed.*, 59: 191–198.
30. Wright, E.H.M. and Pratt, N.C. (1974) Solid/solution interface equilibria for aromatic molecules adsorbed from non-aromatic media. *J. Chem. Soc. Faraday Trans.*, 170: 1461.
31. Ramakrishna, K.R. and Viraraghavan, T. (1997) Use of slag for dye removal. *Waste Management*, 17: 483–488.
32. Rodríguez-Reinoso, F. (1998) The role of carbon materials in heterogeneous catalysis. *Carbon.*, 36: 159–175.
33. Garg, V.K., Kumar, R., and Gupta, R. (2004) Removal of malachite green dye from aqueous solution by adsorption using agro-industry waste: a case study of prosopis cineraria. *Dyes Pigm.*, 62: 1–10.
34. Lagergren, S. (1898) About the theory of so-called adsorption of soluble substances. (Zur Theorie der Sogenannten Adsorption Geloster Stoffe). Kungliga Svenska Vetenskapsakademiens. *Handlingar, Band.*, 24: 1–39.
35. Tütem, E., Apak, R., and Ünal, ÇF. (1998) Adsorptive removal of chlorophenols from water by bituminous shale. *Water Res.*, 32: 2315–2324.
36. Mellah, A., Chegrouche, S., and Barkat, M. (2006) The removal of uranium (VI) from aqueous solutions onto activated carbon: kinetic and thermodynamic investigations. *J. Colloid Interface Sci.*, 296: 434–441.

37. Leitão, A., Conceição, E., Santos, R., and Rodrigues, A. (1992) Modelling of solid-liquid adsorption: effect of adsorbent loads on model parameters. *Can. J. Chem. Eng.*, 70: 690–698.
38. Crank, J. (1975) *The Mathematics of Diffusion*; Clarendon Press: Oxford, U.K.
39. Do, D.D. (1998) *Adsorption Analysis: Equilibria and Kinetics. Series on Chemical Engineering*; Imperial College Press: London, U.K., Vol. 2.
40. Calleja, G., Serna, J., and Rodríguez, J. (1993) Kinetics of adsorption of phenolic compounds from wastewater onto activated carbon. *Carbon*, 31: 691.